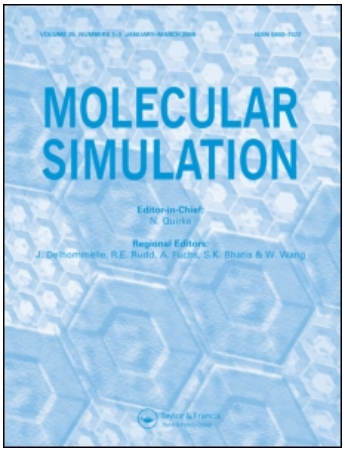


**Molecular Simulation**
Publication details, including instructions for authors and subscription information:
http://www.informaworld.com/smpp/title~content=t713644482

# Liquid state theory of the structure and phase behaviour of polymer-tethered nanoparticles in dense suspensions, melts and nanocomposites

Arthi Jayaraman[a]; Kenneth S. Schweizer[b]
[a] Department of Chemical and Biological Engineering, 424 UCB, University of Colorado, Boulder, CO, USA [b] Department of Materials Science and Engineering and Materials Research Laboratory, University of Illinois, Urbana, IL, USA

**To cite this Article** Jayaraman, Arthi and Schweizer, Kenneth S.(2009) 'Liquid state theory of the structure and phase behaviour of polymer-tethered nanoparticles in dense suspensions, melts and nanocomposites', Molecular Simulation, 35: 10, 835 — 848
**To link to this Article: DOI:** 10.1080/08927020902744680
**URL:** http://dx.doi.org/10.1080/08927020902744680

*Molecular Simulation*
Vol. 35, Nos. 10–11, September 2009, 835–848

Taylor & Francis
Taylor & Francis Group

# Liquid state theory of the structure and phase behaviour of polymer-tethered nanoparticles in dense suspensions, melts and nanocomposites

Arthi Jayaraman[a]* and Kenneth S. Schweizer[b]

[a]*Department of Chemical and Biological Engineering, 424 UCB, University of Colorado, Boulder, CO 80309, USA;* [b]*Department of Materials Science and Engineering and Materials Research Laboratory, University of Illinois, 1304 West Green Street, Urbana, IL 61801, USA*

(*Received 13 December 2008; final version received 8 January 2009*)

We have studied the structure and phase behaviour of spherical nanoparticles grafted with a modest number of polymer tethers in the dense suspension and pure melt states, and dissolved in a homopolymer matrix, using the polymer reference interaction site model integral equation theory. In the absence of a polymer matrix, fluids of tethered nanoparticles exhibit strong concentration fluctuations indicative of aggregate formation and/or a tendency for microphase separation as the total packing fraction and/or nanoparticle attraction strength increase. For nanoparticles of core diameter twice that of the monomer, carrying one, two and four tethers, the microphase spinodal temperature grows roughly as a power-law function of packing fraction. As the number of polymer tethers increases, the microphase spinodal curve shifts to lower temperatures due to steric shielding of the nanoparticle core. In the presence of a homopolymer matrix, the microphase spinodal curve of single-tethered particles exhibits both dilution-like and depletion-like features and a non-monotonic dependence of the spinodal temperature on matrix chain length. As the number of tethers is increased, the microphase curves become more dilution-like and the effect of matrix degree of polymerisation, particle size and tether length on the apparent spinodal temperature diminishes.

**Keywords:** liquid-state theory; polymer-grafted nanoparticles; nanocomposites



## 1. Introduction

Polymer nanocomposites (PNC) [1,2] are composed of nanoparticle additives ('fillers') embedded in a polymer matrix. They offer a variety of enhanced thermal, mechanical, optical and electronic properties relative to pure polymeric materials due to interactions between fillers and the polymer matrix. These enhanced properties make them ideal materials for numerous automotive, aerospace, food packaging and environmental applications. It is well accepted that rational control of spatial organisation of the fillers (dispersion or assembly) is critical for the resultant enhancement of the properties. In the past few years, several research groups have focused on ways to modify the surface of nanoparticle fillers in an effort to improve their dispersion in a polymer matrix. For example, experimentalists have synthesised nanoparticles grafted with polymers having the same chemistry as the matrix polymer at high surface grafting densities [3–5]. They found that these highly grafted nanoparticles disperse (aggregate) if the molecular weight of matrix polymer is lower (higher) than that of grafted polymer [3]. More recently, the focus has shifted from nanoparticles with high surface grafting densities to nanoparticles grafted with a relatively small and controlled number of synthetic grafted polymers [6–9], such as single-tethered CdTe quantum dots [7], gold nanoparticles with a single polyethylene oxide tether [10], and fullerenes end capped with polymethylmethacrylate [11]. Computational [12–18] and theoretical studies [19–21] have shown that pure solutions and melts of these lightly grafted nanoparticles can assemble into a variety of nanostructures, such as sheets, wires and cylinders, with potential applications in photonics and electronics [22], energy storage [23] and chemical and biological sensors [24,25]. Virtually, all studies have focused on solutions of polymer-tethered nanoparticles, and little is known about the behaviour of this new class of hybrid fillers in PNC.

In recent work [20,21,26], we generalised and applied the microscopic polymer reference interaction site model (PRISM) liquid-state theory [27,28] to study concentrated solutions and melts of one- [20], two- and four- [21] tethered spherical nanoparticles, and also composites composed of single- and two-tethered nanospheres in a homopolymer matrix [26]. In the absence of a polymer matrix, despite the seeming simplicity of the one or two polymer tether(s) plus sticky nanoparticle system, a rich physics emerges due to competing entropic and enthalpic effects and asymmetric excluded volume interactions. For example, there is a competition between the polymer-mediated entropic depletion-like attraction between nanoparticle cores and steric stabilisation due to tether–tether repulsion. Direct nanoparticle attractions favour

*Corresponding author. Email: arthi.jayaraman@colorado.edu

ISSN 0892-7022 print/ISSN 1029-0435 online

DOI: 10.1080/08927020902744680
http://www.informaworld.com

particle clustering and assembly, in a manner that can be strongly modified by the attached polymer chain. Moreover, the direct nanoparticle attraction can, in principle, induce either macro- or microphase separation. Our theoretical studies find that fluids of such hybrid nanoparticles show strong concentration fluctuations indicative of aggregate formation and/or a tendency for microphase separation as the total packing fraction and/or nanoparticle attraction strength increase. In the presence of a polymer matrix of chemical structure identical to the grafted chains, there is a competition between tether-induced steric stabilisation, which can induce microphase ordering, and matrix-induced depletion attraction, which can drive macrophase separation.

PRISM theory provides all the intermolecular pair correlation functions and partial collective structure factors over all length and wave vector scales. It also yields the very high wave vector correlation function information, which is critical input to modern dynamical theories of kinetic arrest and solid (glass and gel) elastic properties [29–31]. Another significant advantage of using the theory is that it is computationally much less demanding than a full simulation approach, which is especially important for systems at high volume fractions that are our primary interest. Of course, computer simulations have the powerful advantages of being essentially exact and of possessing the capability to predict and visualise ordered phases. The latter stands in contrast to homogeneous phase PRISM theory, which describes only a generic tendency for microphase separation. Such a limitation can potentially be relaxed by combining the liquid-state structural information obtained from PRISM theory with thermodynamic density functional methods [29,32].

In this paper, we discuss the recent applications of PRISM theory for polymer-tethered nanoparticles as melts and fillers in PNC. In Section 2, the model and theory are summarised. Section 3 presents highlights of our study of concentrated solutions and melts of nanoparticles with one-, two- and four-polymer grafts. Representative results for one- and two-tethered nanoparticles dissolved in a homopolymer matrix are discussed in Section 4. The paper concludes in Section 5 with a discussion and future outlook.

## 2. Model and theory

### 2.1 Model and interaction potentials

The tethers and matrix homopolymers are treated as freely jointed chains of $N_p$ and $N_m$ spherical interaction sites (monomers), respectively. The monomers, of diameter $d$, are connected by a rigid bond of length $l = 1.4d$ (a typical persistence length), where $d \equiv 1$ is the unit of length. The polymer tethers are permanently grafted on rigid nanospheres of diameter $D$. The subscripts 'p', 'c' and 'm' denote tether polymer, nanoparticle and matrix polymer, respectively. The total fluid packing fraction is $\eta$, and the fraction of $\eta$ composed of polymer-tethered particles is the mixture composition variable, $\phi$. Calculations in the absence of a polymer matrix correspond to $\phi = 1$, while decreasing values of $\phi$ correspond to mixtures of increasing fraction of homopolymer matrix. A schematic of the model systems is shown in Figure 1(a),(b).

The site–site pair decomposable interactions between tether monomers (or segments), $U_{pp}$, tether monomers and nanoparticles, $U_{pc}$, matrix monomers, $U_{mm}$, matrix and tether monomers, $U_{mp}$, and matrix monomer and nanoparticles, $U_{mc}$, all include a hard core repulsion. The only attractive interactions in the present paper are between nanoparticles, $U_{cc}$, modelled beyond contact as the attractive branch of the colloid Lennard-Jones (CLJ) potential [33]. The CLJ potential describes the interaction between two nanospheres as a pair wise sum over LJ potentials between elementary units of size b. An example of the attractive branch of the CLJ potential for a tethered particle with $D = 2b$ and $b = d$ [20] is shown in Figure 1(c); its strength is characterised by the value at contact, $-\varepsilon_{cc}$.

Our choice of model and interactions are meant to mimic a real system, where the nanoparticle–homopolymer and homopolymer–homopolymer attractions are weak and very similar, and nanoparticles have a different chemistry from the homopolymer chains, resulting in unbalanced van der Waals attractions between them, which can be strong relative to the thermal energy. In the presence of a polymer matrix ($\phi < 1$), the model mimics a PNC composed of homopolymer-tethered nanoparticles dissolved in a homopolymer melt, where the matrix and tether polymers are the same chemistry.

### 2.2 Polymer reference interaction site model theory

PRISM is an equilibrium theory that describes well the structure of both suspensions and dense melts composed of hard spherical particles and linear chains [20,34–37]. The theory is based on the Ornstein–Zernike-like matrix or Chandler–Andersen integral equations [38] that relate the total site–site intermolecular pair correlation function between different sites, $h_{ij}(r) = g_{ij}(r) - 1$, to the site–site intermolecular direct correlation function, $C_{ij}(r)$, and intramolecular probability distribution functions, $\omega_{ij}(r)$. The matrix PRISM equations in Fourier space are

$$\underset{\sim}{H}(k) = \underset{\sim}{\Omega}(k)\underset{\sim}{C}(k)[\underset{\sim}{\Omega}(k) + \underset{\sim}{H}(k)], \tag{1}$$

$$H_{ij}(k) = \rho_i \rho_j h_{ij}(k), \tag{2a}$$

$$\Omega_{ij}(k) = \rho \sum_{\alpha=1}^{N_i} \sum_{\beta=1}^{N_j} \omega_{\alpha i \beta j}(k). \tag{2b}$$

Here, $i$ and $j$ are two types of interaction sites, $N_i$ is the number of interaction sites of type $i$, $\rho_i = N_i \rho$ the total site

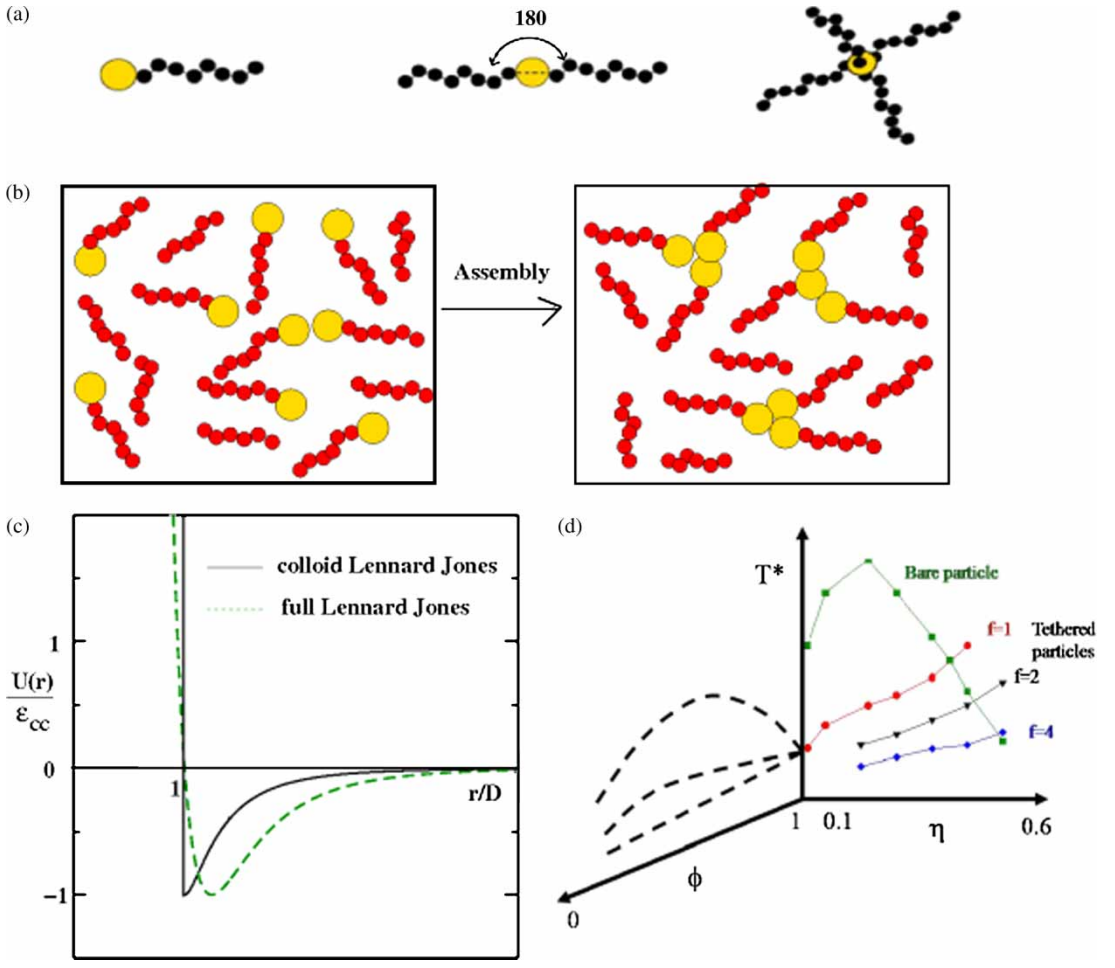


Figure 1. (a) Schematic of the model system of polymer-tethered nanoparticles with one, two and four tethers. (b) Schematic of single-tethered nanoparticles embedded in a polymer melt undergoing cluster formation and higher level ordering. (c) CLJ potential $U(r)$ (black solid curve) as a function of $r/D$ with $D/b = 2$, and standard LJ potential (green dashed curve). All potentials are normalised to $-1$ at the depth of their respective attractive minimum. (d) Schematic of the microphase spinodal temperature, $T^*$, as a function of total fluid packing fraction ($\eta$) and filler volume fraction ($\phi$). Reprinted with permission from [26]. Copyright (2008) American Chemical Society.

density of species $i$, and $\rho$ the molecular number density. For dense solutions (implicit solvent) and melts [20,21] of polymer-tethered nanoparticles, $\underline{H}(k)$, $\underline{C}(k)$ and $\underline{\Omega}(k)$ are $2 \times 2$ matrices associated with the correlations of two types of sites, 'c' and 'p'. For polymer-tethered nanoparticles in a homopolymer matrix, $\underline{H}(k)$, $\underline{C}(k)$ and $\underline{\Omega}(k)$ are $3 \times 3$ matrices describing the correlations of three types of sites, 'c', 'p' and 'm'. In all our studies, explicit chain end effects are ignored (pre-averaged) as in prior applications of PRISM theory to homopolymers [27,28], PNC [34–37] and block copolymers [39–43]. Explicit equations for $h_{ij}(k)$, the intramolecular pair correlation function $\omega_{ij}(k)$, and the partial collective structure factors, $S_{ij}(k)$, are given in [20,21,26].

In our studies to date, possible non-ideal conformational perturbations of the tether and matrix polymers have been ignored. In principle, they can be treated using the fully self-consistent and more computationally intensive version of PRISM theory, which involves a medium-induced solvation potential and solution of an effective single-chain problem via Monte Carlo simulation [28,44]. However, the construction and testing of such a solvation potential for tethered particles in a polymer melt is presently an unsolved problem. Moreover, we expect chain stretching or contraction effects to be most important in dilute solutions and/or when particle–polymer or polymer–polymer interactions are attractive. Our present focus is melt-like packing fractions and polymer-related attractions are absent, conditions, where conformational non-idealities of excluded volume and enthalpic origin are expected to be minimised. In addition, we do not consider long tethers, which should also mitigate large non-ideal conformational effects, and minimise unphysical intra-chain overlaps present in any ideal chain model [28].

Approximate closure relations are required to solve the coupled PRISM integral equations. For PNC, the

site–site Percus–Yevick (PY) closure [27,28,34,37,38] is quite accurate for all direct correlation functions except particle–particle. Previous PNC studies have shown that the hypernetted chain (HNC) approximation [34] is a good closure for the particle–particle direct correlation function, which also ensures that the physical condition $g_{cc}(r) > 0$ holds for all $r$. If $\sigma_{ij}$ is the distance of the closest approach between sites of type $i$ and $j$, the hard core impenetrability conditions are

$$g_{ij}(r) \equiv 0, \quad r < \sigma_{ij}. \tag{3}$$

Outside the hard core the site–site PY approximation [27,28,34,38] is employed for all, except particle–particle, direct correlations

$$C_{ij}(r) = \left(1 - e^{\beta U_{ij}(r)}\right) g_{ij}(r), \quad r > \sigma_{ij} \tag{4}$$

and the HNC closure [29,36] is adopted for the particle–particle direct correlation function

$$C_{cc}(r) = h_{cc}(r) - \ln g_{cc}(r) - \beta U_{cc}(r), \quad r > \sigma_{ij}. \tag{5}$$

For the single-tethered nanoparticle system [20] quite good agreement with simulation [14] has been demonstrated, which supports the usefulness of these atomic closures. We note that for polymer blends and block copolymers composed of monomers of (nearly) the same size, the so-called 'molecular closures' are the most accurate [28]. Whether such closures are better for PNC with hybrid nanoparticles is unknown. To efficiently solve the coupled nonlinear integral equations the Kinsol algorithm [45] is employed, which is based on the inexact Newton's method and has a relatively high ease of convergence, especially compared with Picard algorithm [34]. Numerical solution of the PRISM equations yields the intermolecular pair correlation functions, $g_{ij}(r)$, and partial collective structure factors, $S_{ij}(k)$. The potential of mean force (PMF) between nanoparticles, $W_{cc}(r)$, follows as

$$W_{cc}(r)/k_B T = -\ln [g_{cc}(r)]. \tag{6}$$

### 2.3 System parameters

There are many controllable material parameters: tether polymer degree of polymerisation, $N_p$, number of polymer tethers, $f$, placement of tethers on the nanoparticle surface, ratio of particle-to-monomer diameter, $D/d$, matrix polymer degree of polymerisation, $N_m$, total fluid packing fraction, $\eta$, fraction of $\eta$ composed of tethered particles, $\phi$, and absolute magnitude of the particle–particle attraction strength in units of the thermal energy, $\varepsilon_{cc}$. Most calculations presented here are for tethered particles with $N_p = 8$ and 27, $f = 1$, 2, 4 and 6 and $D/d = 2$ and 3, and polymer matrix lengths ranging from $N_m = 1$ ('solvent') to 50. The values $N_p = 8$ and $D/d = 2$ are chosen to ensure that the volume of the particle equals to the total volume of the tethers. For the results presented in this paper, the grafted chain on the two-tethered nanoparticles are symmetrically placed 180° apart. More generally, the two grafted chain placement can be varied, and angles of 60°, 90° and 120° have been studied [21]. For the four-tethered nanoparticles, the grafted chains are placed in a symmetric tetrahedral arrangement on the particle (a symmetric equatorial square planar arrangement was also studied in [21]). We also present a few results for $f = 6$, where the tethers are placed symmetrically on the filler surface. In all cases, the attachment points are fixed corresponding to a 'quenched' (not annealed) grafting process. The attraction strength $\varepsilon_{cc}$ is varied from 0 (athermal) to several kT. The total packing fraction, $\eta$, is varied from 0.3 to 0.5 representative of a dense melt or concentrated solution, and $\phi$ is varied from 1 (pure melt of tethered particles) to 0 (pure homopolymer matrix).

### 2.4 Phase behaviour

PRISM theory describes the correlated and spatially segregated, but globally homogeneous, fluid states. It is not a mean field theory, and includes concentration fluctuations on all length scales. Literal spinodal instabilities at non-zero wave vectors (structure factor divergences at $k^*$) are not predicted [39–43]. However, in extensive prior applications of the theory to diblock [28,39–43] and multiblock [46,47] copolymers, an analysis of small-angle scattering profiles was proposed, which allows a useful estimate of a microphase separation transition in the sense of an extrapolated spinodal instability. In polymer (mean) field theories and experimental scattering analyses, the quantity $1/S_{cc}(k^*)$ is taken as an order parameter which would vanish at a literal spinodal instability [48,49]. We estimate the spinodal instability via linear extrapolation of $1/S_{cc}(k^*)$ as a function of the inverse dimensionless temperature, $1/T^*$. When applied to melts of single-tethered particles [20], the resulting microphase spinodal curve was shown to be in good agreement with the order–disorder boundary obtained using simulations by Iacovella et al. [14] This motivates an analogous analysis of the tethered particles in the presence of homopolymer matrix.

A schematic of the microphase spinodal temperatures, $T^*$, versus total packing fraction, $\eta$, and volume fraction of tethered particles, $\phi$, phase diagram is shown in Figure 1(d). A question of high interest is how the microphase spinodal curves for the polymer-tethered nanoparticles change as $\phi$ decreases (amount of polymer matrix increases). Section 3 discusses dense solutions and melts of polymer-tethered nanoparticles in the absence of a homopolymer matrix ($\phi = 1$), followed by a presentation of results for tethered nanoparticles as fillers in a PNC ($\phi < 1$) in Section 4.

## 3. Melts and dense solutions of polymer-tethered particles

### *3.1 Athermal conditions*

In the athermal or purely entropic limit, polymer tether-mediated depletion-like attraction and steric stabilisation effects associated with excluded volume interactions compete in the absence of energetic biases. Figure 2 presents results for the collective particle–particle structure factor, $S_{cc}(k)$, particle–particle pair correlation function, $g_{cc}(r)$, and PMF, $W_{cc}(r)$, (as insets) for nanoparticles of size $D/d = 2$ with a single tether ($f = 1$), two tethers ($f = 2$), and four tethers ($f = 4$) of length $N = 8$, at packing fractions $\eta = 0.1$, 0.2, 0.5 and 0.6.

For the nanoparticles with a single polymer tether [20], a weak small-angle 'microphase' peak in $S_{cc}(k)$ (Figure 2(a)) emerges at a very high packing fraction of $\eta = 0.5$. For two tethers (Figure 2(b)), a small-angle peak is visible only at an even higher packing fraction of $\eta = 0.6$, and is much weaker compared with the single tether analogue. For four tethers (Figure 2(c)) there is no small-angle peak. Hence, under athermal conditions, the tendency to microphase separate is always very weak, and decreases as the number of tethers increases due to reduced steric anisotropy of the particle. The wide-angle peak in $S_{cc}(k)$ shifts to higher wave vector as packing fraction increases indicating that the tethered particles are pushed together closer. At fixed $\eta$, the nanoparticle local cage order, as quantified by the intensity of the wide-angle peak, also decreases strongly with increasing number of tethers.

For all three systems, the real space $g_{cc}(r)$ displays a growth of the contact value as $\eta$ increases (Figure 2(d)–(f)), which decreases as the number of tethers grows due to increased steric repulsion. For the single tether case (Figure 2(d)), there is no noticeable peak at any other interparticle separation. By contrast, for two tethers (Figure 2(e)), as packing fraction increases two additional peaks in $g_{cc}(r)$ develop at $r/D = 1.5$ and 2, and for four tethers (Figure 2(f)) three additional peaks develop at $r/D = 1.25$, 1.65 and 2.2. This suggests that under athermal high $\eta$ conditions, as the number of tethers increases the particles are effectively pushed apart and locally order at larger interparticle separations.

The insets in Figure 2(d)–(f) show the PMF calculated at $\eta = 0.2$ and 0.5. For single-tethered particles [20] in the infinite dilution limit the PMF is always repulsive (not shown). However, as the packing fraction increases from 0.1 to 0.6 (Figure 2(d)) the nanoparticle PMF changes from repulsive to strongly attractive at contact, indicating a muted form of entropy-driven depletion attraction of many body origin. For two-tethered particles (Figure 2(d)), as the packing fraction increases from 0.2 to 0.5 the PMF changes from repulsive to slightly attractive at contact. Four-tethered particles have a repulsive PMF at both packing fractions. Hence, as the number of tethers increases (or the degree of overall particle anisotropy decreases) a higher fraction of the particle surface is shielded by the grafted chains. This enhances the effective steric repulsion between particle cores, which is the expected classic behaviour in the high grafting limit.

### *3.2 Effect of particle–particle attraction strength*

We now consider the same $f = 1$, 2 and 4 and $N = 8$ tether systems as in the previous section but in the presence of direct particle–particle attractions of variable contact strength $\varepsilon_{cc}$ (in units of the thermal energy, kT). The packing fraction is fixed at the concentrated solution or melt-like value of $\eta = 0.30$. The direct attraction between the particles can potentially induce macrophase separation, or strong aggregate formation and subsequent microphase type ordering. In analogy with block copolymer assembly in solution and the melt [49], the latter situation can be viewed as indicating large concentration fluctuations [48,50], and perhaps a hierarchical assembly, where relatively small aggregates or micelles first form, which then organise as a highly correlated liquid [51,52]. As true for the experimental analysis of scattering curves, the theory is limited in the level of spatial organisation that can be deduced based on ensemble-averaged pair correlation functions. However, the theory does provide all three real and Fourier space correlations functions over all length scales.

Prior simulation work [14] and self-consistent field studies of tadpole particles [19] have demonstrated that microphase separation can occur for lightly tethered nanoparticles. However, the general question of whether long-range ordering can be achieved as the nanoparticle size and number and length of tethers are varied, or only finite clusters are formed, or the system remains a correlated fluid of single hybrid particles, is not *a priori* obvious. The direct particle–particle attraction favours cluster formation and potentially microphases, since macroscopic phase separation is frustrated due to inter-tether excluded volume interactions. In addition, at high volume fractions, inter-tether excluded volume interactions can potentially mediate a weak form of depletion attraction, which favours close nanoparticle contact since it enhances tether conformational entropy. However, this effect competes with the direct repulsions between tethered chains that tend to push nanoparticles apart (steric stabilisation). For lightly tethered particles, the energy-entropy competition can be subtle. Specifically, whether the grafted chains mediate attraction and/or repulsion in the nanoparticle PMF depends on fluid packing fraction, the number and length of tethers and, in principle, their precise placement. As the number of tethers increases, their intermolecular repulsion monotonically suppresses entropy-driven nanoparticle aggregation and increasingly frustrates clustering and

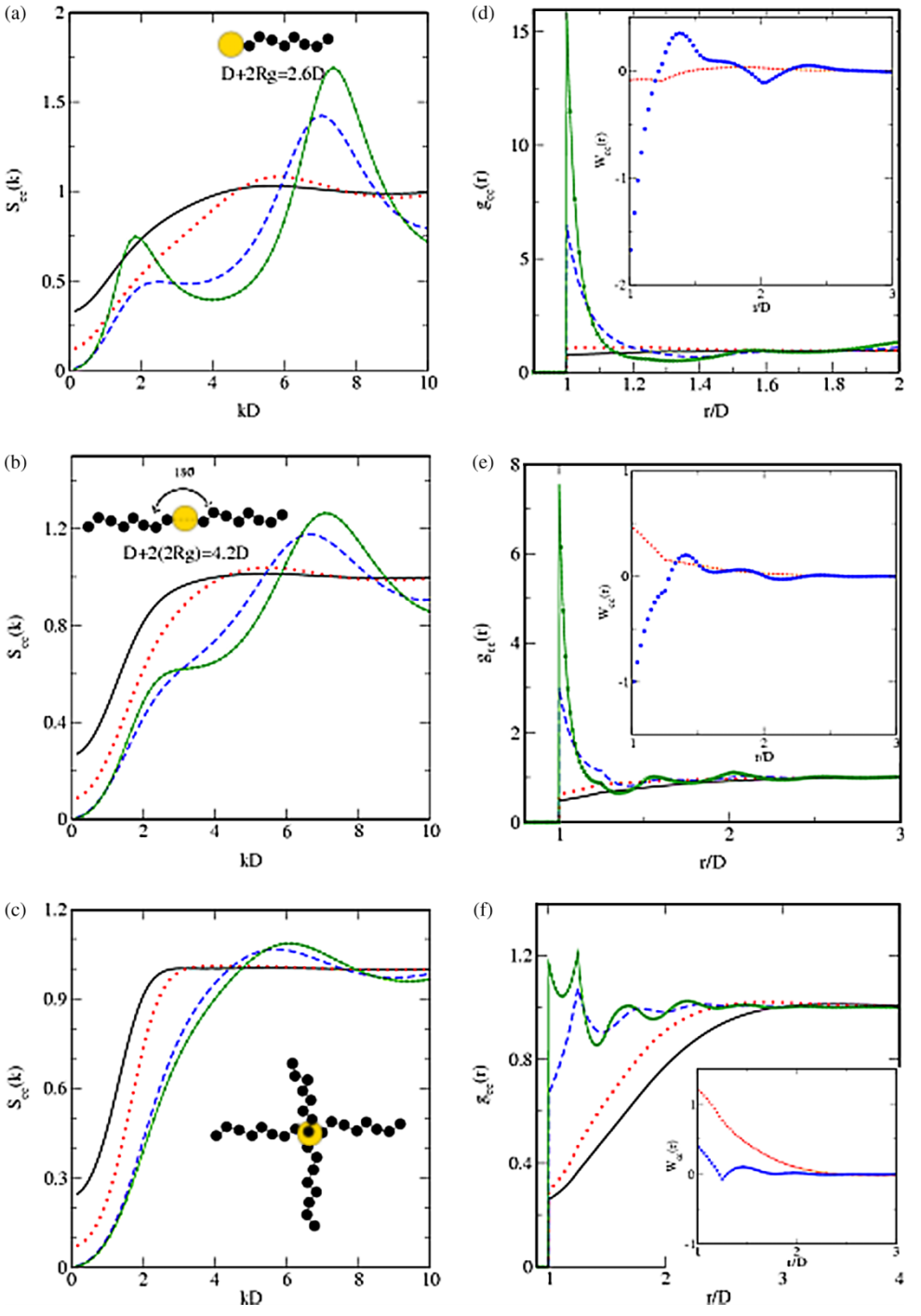


Figure 2. Particle–particle collective structure factor, $S_{cc}(k)$, and the corresponding pair correlation function, $g_{cc}(r)$, for single tether [(a) and (d)], two tethers placed at 180° [(b) and (e)], and four tethers placed tetrahedrally [(c) and (f)] on a particle of size $D = 2d$ with tether length $N = 8$, at total fluid packing fractions of 0.1 (solid line), 0.2 (dotted line), 0.5 (dashed line) and 0.6 (cross-solid line) under athermal conditions. The insets show the PMF $W_{cc}(r)$ at packing fractions 0.2 (dotted line) and 0.5 (dashed line). Reprinted with permission from [21]. Copyright (2008) American Chemical Society.

microphase separation, resulting in a reduction of the apparent microphase separation temperature. Moreover, we expect (and have found) that asymmetric placement of multiple tethers reduces the excluded volume-induced repulsion between nanoparticle cores.

Figure 3 presents structural results for increasing attraction strengths and nanoparticles of size $D/d = 2$ with a single tether, two tethers (placed at 180°) and four tethers (placed tetrahedrally) of length $N_p = 8$. For nanoparticles with a single tether, Figure 3(a) shows that

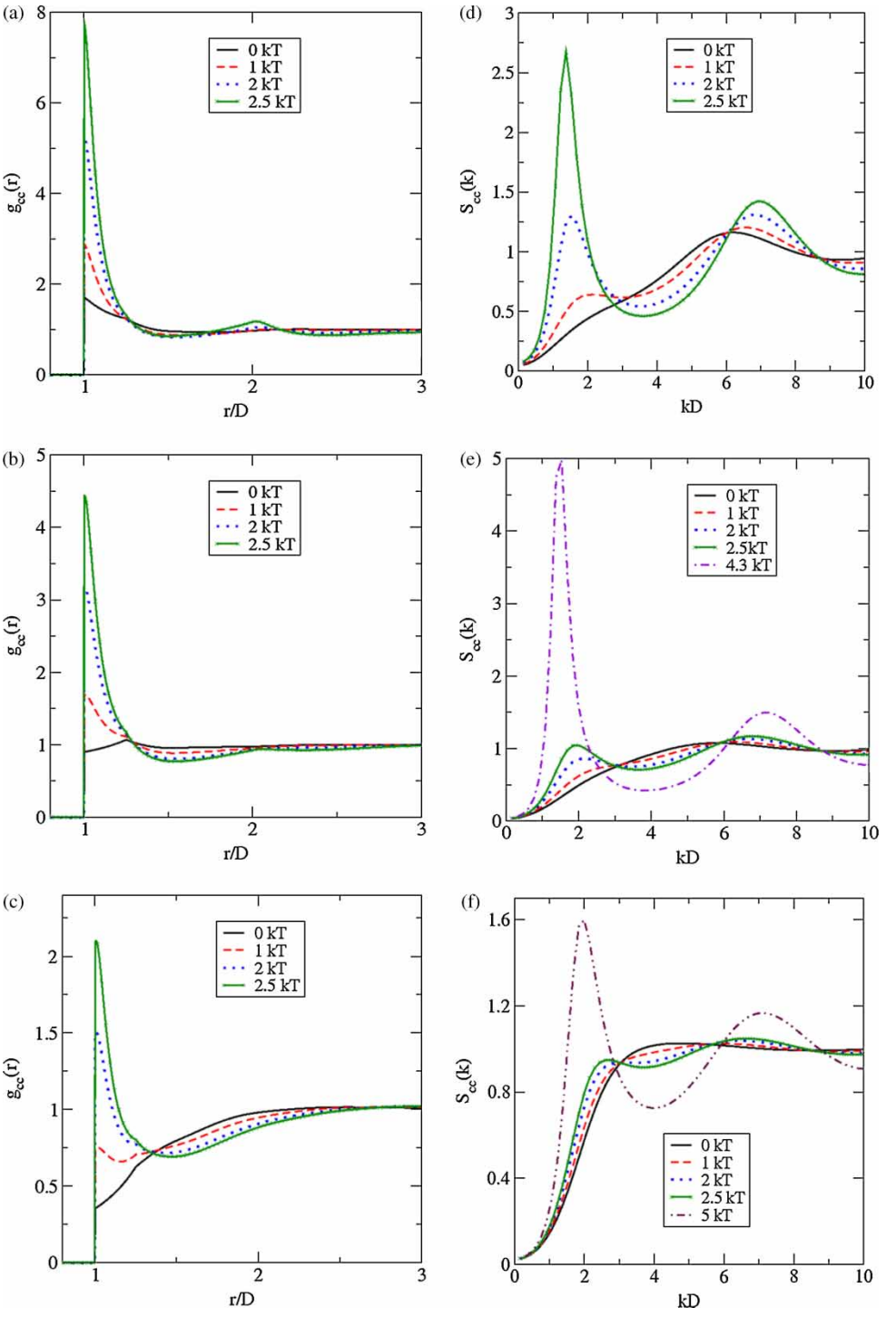


Figure 3. Particle–particle pair correlation function, $g_{cc}(r)$, and structure factor, $S_{cc}(k)$, for single tether [(a) and (d)], two tethers placed at 180° [(b) and (e)], and four tethers placed tetrahedrally [(c) and (f)] on a particle of size $D = 2d$ with tether length $N = 8$, total fluid packing fraction = 0.3 and particle–particle attraction strength $\varepsilon_{cc} = 0$ (solid line), kT (dashed line), 2 kT (dotted line) and 2.5 kT (cross-solid line). Reprinted with permission from [21]. Copyright (2008) American Chemical Society.

the particle–particle pair correlation function has a peak at contact, and a second smaller peak at $r/D = 2$, as $\varepsilon_{cc}$ increases from zero to 2.5 kT. The corresponding structure factor $S_{cc}(k)$ (Figure 3(d)) develops a small-angle microphase peak, which rapidly intensifies as $\varepsilon_{cc}$ grows. For particles with two tethers, $g_{cc}(r)$ (Figure 3(b)) exhibits a much lower contact peak, and the small-angle microphase peak in $S_{cc}(k)$ (Figure 3(e)) grows and sharpens as $\varepsilon_{cc}$ increases.

For particles with four tethers, the contact value of $g_{cc}(r)$ and small-angle peak in $S_{cc}(k)$ are even smaller than the corresponding two tether case (Figure 3(c),(f)). It is interesting to compare the different tether systems at the same $\eta$ and $\varepsilon_{cc}$. As the number of tethers increase the small-angle peak in $S_{cc}(k)$ decreases, suggesting that more grafted chains frustrate nanoparticle ordering. This trend is corroborated by the real space $g_{cc}(r)$, where as the number of tethers increase the contact value decreases. In addition, the single tether system has a peak at $r/D = 2$, while there are no additional peaks in $g_{cc}(r)$ for $f = 2$ and 4, and a correlation hole develops that deepens as $f$ and $\varepsilon_{cc}$ increase.

The position of the small-angle peak in $S_{cc}(k)$ is related to the microphase-like periodicity. As the number of tethers increases, the location of the small-angle peak non-dimensionalised by the nanoparticle diameter, $k^*D$, shifts to higher wave vectors (Figure 3(d)–(f)). Specifically, $k^*D \sim 1.2$, 1.5 and 2 for $f = 1$, 2 and 4, respectively. The corresponding length scales, $2\pi/k^*$, are $5.2D$, $4.2D$ and $3.14D$, respectively. These length scales can also be related to the effective size of the tethered particles as discussed in [21].

The sharp peak of $S_{cc}(k)$ and $S_{pp}(k)$ at a non-zero wave vector ($k^* \neq 0$) that rapidly grows as $\varepsilon_{cc}$ increases suggests that the system is approaching a microphase separation transition. Alternatively, a sharp increase at $k^* = 0$ indicates macrophase demixing. In polymer (mean) field theories and experimental scattering analyses, the quantity $1/S_{cc}(k^*)$ is taken as an order parameter, which would vanish at a literal spinodal instability [49,52]. From a plot of the inverse microphase order parameter, $1/S_{cc}(k^*)$, at various packing fractions (as shown in Figure 4(a) for single-tethered particles) we estimate via linear extrapolation an apparent microphase spinodal and the corresponding value of $\varepsilon_{cc}$, as discussed in Section 2.4. As seen in the case of single-tethered particles shown in Figure 4(a), the $1/S_{cc}(k^*)$ versus $\varepsilon_{cc}$ curves show a linear region at low $\varepsilon_{cc}$ (high temperatures), but 'bends up' at high $\varepsilon_{cc}$ (low temperatures) for all cases due to 'fluctuation stabilisation' similar to the behaviour seen in block copolymers [40,53].

In Figure 4(b), the spinodal curve, $T^*$ versus $\eta$, is plotted for all three systems. At a constant packing fraction, as the number of tethers increases the extrapolated spinodal transition temperature ($1/\varepsilon^*_{cc}$) decreases. For example, at $\eta = 0.3$ we find $T^* = 1/\varepsilon^*_{cc} \sim 0.34$, 0.22 and 0.14 for one, two and four tethers, respectively. As $f$ increases from 1 to 4 the microphase spinodal curves shift to lower temperatures because the tethers sterically frustrate nanoparticle clustering. For one-component simple fluids, crystallisation occurs at a nearly constant value of $S(k^*) \sim 2.85$, an empirical criterion known as the 'Verlet–Hansen rule'. The corresponding Verlet–Hansen temperatures for our systems (dashed lines) are shown along with the macrophase spinodal curve for systems containing bare spheres of size $D/d = 2$ with no tether. For all three systems, the Verlet–Hansen curves lie above (higher temperature) the spinodal analogue, qualitatively consistent with the idea that it is an indication of a first-order microphase transition. For single-tethered particles [20] $T^* \propto \eta^{0.38}$, which is far weaker than the experimental behaviour of diblock copolymers in good (athermal) solvents [54], where $T^{ODT}$(order disorder transition) $\propto \eta^{1.6}$. This very different dependence on packing fraction presumably arises from the large excluded volume asymmetry of the tethered nanosphere compared with a diblock copolymer composed of linear chains. For two tethers the best power-law fit of our calculations is $T^* \propto \eta^{0.63}$, while for four tethers $T^* \propto \eta^{0.54}$. Hence, the dependence of $T^*$ on $\eta$ is different for the three tether number cases, and always much weaker than the diblock copolymer in a good solvent analogue. We have also compared our microphase spinodal calculations with a recent simulation of the phase behaviour of single-tethered $D/d = 2$ spherical nanoparticles by Glotzer and coworkers [14] and found the agreement to be surprisingly good as discussed in [20].

For the $D/d = 3$ system of single-tethered nanoparticles (not shown here [20,21]), $T^*$ is nearly independent of packing fraction over the wide range $\eta = 0.15$–$0.5$. This is remarkably different than the behaviour of the $D/d = 2$ system, where $T^*$ monotonically increases with $\eta$. Furthermore, the microphase spinodal temperatures for $D/d = 3$ lie below the $D/d = 2$ analogues, and at high $\eta$ are quantitatively close to the macrophase separation of the particles with no tether. These differences reflect the decreased grafted chain-mediated driving force for microphase ordering, and enhanced tendency for macrophase separation, for the larger nanoparticle system.

## 4. Polymer-tethered particles in a homopolymer matrix

Earlier work on athermal PNC [36,37,55] has shown that a melt of free chains induces a strong entropic depletion attraction between nanoparticles resulting in filler macrophase separation. For the case of lightly tethered attractive nanoparticles in a polymer matrix, there are potentially three qualitatively different organisational scenarios that can arise due to the competition between nanoparticle–nanoparticle attractions, steric repulsion between grafted tethers, and filler-homopolymer mixing considerations including the depletion-like entropic attraction. (i) Strong inter-tether repulsions can sterically shield nanoparticle–nanoparticle attractions, and if the depletion effects are weak, then the fillers can form a well-dispersed correlated fluid in the homopolymer matrix. (ii) If inter-tether repulsion is weak, and nanoparticle attractions are strong enough, then the filler attraction plus matrix-induced depletion effects can induce macroscopic phase separation into matrix-rich and tethered nanoparticle-rich coexisting phases. (iii) If nanoparticle–nanoparticle attractions are strong enough relative to the thermal energy, and sufficient steric stabilisation exists due to tether repulsion to preclude

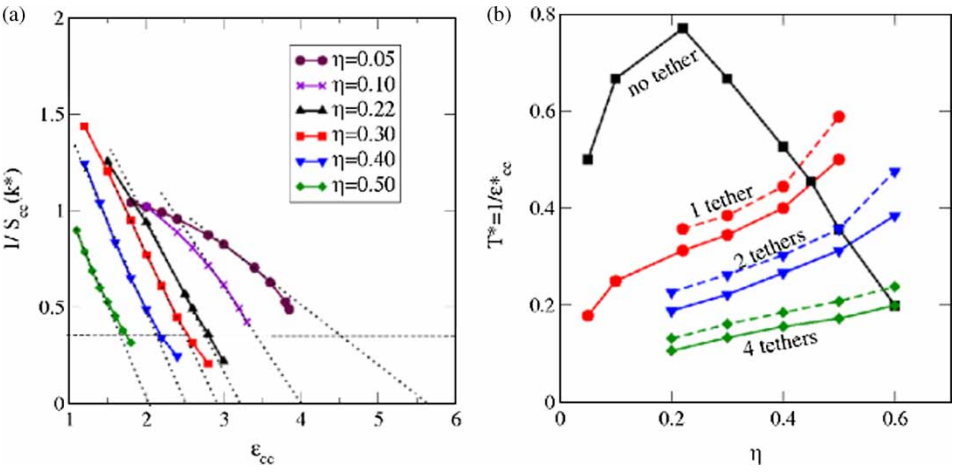


Figure 4. (a) Inverse of the microphase order parameter, $1/S_{cc}(k*)$, as a function of particle–particle attraction strength $\varepsilon_{cc}$ (in units of kT) for a single-tethered nanoparticle of size $D = 2d$ with tether length $N = 8$. Dotted line shows an example of the linear extrapolation to obtain the spinodal $\varepsilon*_{cc}$. Dashed horizontal line corresponds to the Verlet–Hansen rule, $S_{cc}(k*) = 2.85$. (b) Microphase spinodal curves, $T*$ versus $\eta$, for particles of size $D = 2d$ with no tether (macrophase spinodal), one tether, two tethers (placed at 180°) and four tethers (placed tetrahedrally). Also shown are the corresponding Verlet–Hansen temperatures, $T_{VH}$ (dashed lines). Reprinted with permission from [21]. Copyright (2008) American Chemical Society.



macrophase demixing, then stable aggregate formation and/or microphase type of ordering can occur. We have found all three types of behaviour for attractive tethered nanoparticles dissolved in a homopolymer melt of the same chemistry as the grafted chains. The competing physical effects that determine the thermodynamics and structure are functions of the effective nanoparticle attraction strength, tether grafting density and chain length, matrix chain length, total packing fraction and mixture composition.

### *4.1 Athermal conditions*

In Figure 5(a), we present athermal limit calculations of the particle–particle pair correlation function, $g_{cc}(r)$, and collective structure factor, $S_{cc}(k)$, for $D/d = 2$ with $f = 1$ and 2 tethers of length of $N_p = 8$ in a $N_m = 8$ matrix at a packing fraction $\eta = 0.5$ for $\phi = 0.2$, 0.5 and 0.8. For all compositions ($\phi$), as the number of tethers increases from 1 to 2, $g_{cc}(r)$ at contact decreases. The presence of additional peaks at $r/D \sim 1.55$ and 2 suggest weak local ordering beyond contact. The structure factors for $f = 1$ systems have a weak small-angle peak, which is absent for $\eta < 0.5$ (not shown), and two-tethered particles do not exhibit any small-angle peak. All trends imply that as the number of tethers increases nanoparticle clustering is reduced because of enhanced steric repulsion. For both $f = 1$ and 2, as $\phi$ decreases from 0.5 (dotted curve) to 0.2 (solid curve), $g_{cc}(r)$ at contact and the magnitude of the small-angle peak increase. This is because as the fraction of polymer matrix increases, the tethered particles are entropically pushed together due to matrix-induced depletion attraction.

The effect of matrix polymer chain length on the organisation of $f = 1$ and 2 tethered particles is shown in Figure 5(b) for tether length $N_p = 8$ and matrix degree of polymerisation $N_m = 1$, 8 and 50, at fixed $\eta = 0.5$ and $\phi = 0.5$. The local particle order is not very sensitive to $N_m$ under athermal conditions, although the contact values of $g_{cc}(r)$ weakly decrease as $N_m$ increases. Interestingly, this trend is opposite to that found in the case of homopolymer matrix containing relatively large nanoparticles with high surface grafting density [3]. The reason is presumably that classic polymer brush physics is dominant only at high graft densities under locally flat surface ($D/d \gg 1$) conditions, where filler dispersion is governed by entropic wettability considerations [56–58]. For nanoparticles with only one or two polymer tethers, dispersability is likely controlled by the fraction of a filler surface covered by grafted chains and unavailable for nanoparticle contacts. The weak small-angle peak in $S_{cc}(k)$ (inset of Figure 5(b)) for single-tethered particles decreases as $N_m$ increases, and disappears for $N_m = 50$. There are no small-angle peaks for two-tethered nanoparticles. The nanoparticle osmotic compressibility, proportional to $S_{cc}(k = 0)$, grows as $N_m$ increases for both 1 and 2 tether cases.

### *4.2 Effect of particle–particle attraction strength*

Figure 6 presents calculations of $g_{cc}(r)$ and $S_{cc}(k)$ for nanoparticles (size $D/d = 2$) that weakly attract ($\varepsilon_{cc} = kT$) that carry 1 and 2 tethers of length $N_p = 8$ in matrices of chain lengths $N_m = 1$, 8 and 50 at $\eta = 0.5$ and $\phi = 0.5$. At fixed $N_m$, aggregation of the tethered particles decreases as $f$ increases, similar to athermal limit results in Figure 5(b). For both $f = 1$ and 2 the local ordering is similar, with no major effect of matrix polymer chain length on either structure. The inset of Figure 6 shows that

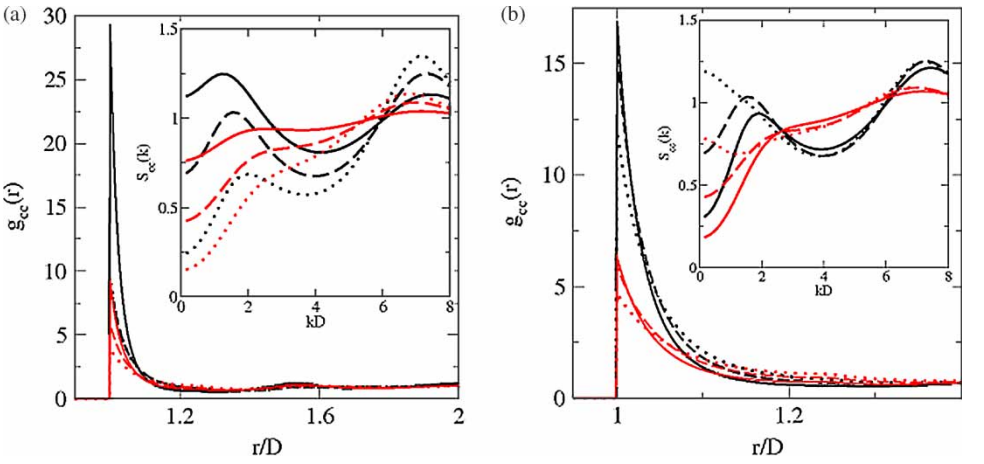


Figure 5. Particle–particle pair correlation function, $g_{cc}(r)$, and collective structure factor, $S_{cc}(k)$, as inset, for nanoparticles under athermal conditions with 1 (black) and 2 (red) tethers of $N_p = 8$, particle size $D/d = 2$, in a homopolymer matrix of variable degree of polymerisation: (a) $N_m = 8$ at a packing fraction $\eta = 0.5$ and $\phi = 0.2$ (solid), 0.5 (dashed) and 0.8 (dotted); (b) $N_m = 1$ (solid), 8 (dashed) and 50 (dotted) at a packing fraction $\eta = 0.5$ and $\phi = 0.5$. Reprinted with permission from [26]. Copyright (2008) American Chemical Society.

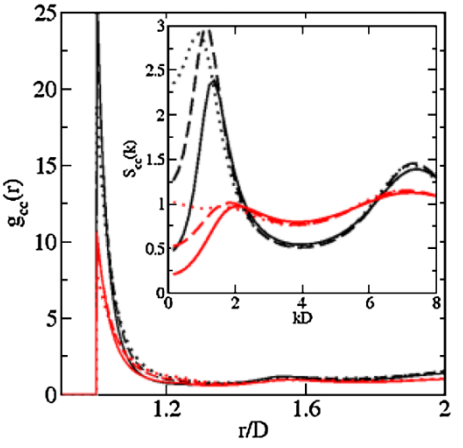


Figure 6. Particle–particle pair correlation function, $g_{cc}(r)$, and structure factor, $S_{cc}(k)$, for tethered nanoparticles with 1 (black) and 2 (red) tethers of $N_p = 8$, particle size $D/d = 2$, in a matrix polymer of degree of polymerisation $N_m = 1$ (solid), 8 (dashed) and 50 (dotted) at a packing fraction $\eta = 0.5$ and $\phi = 0.5$ and $\varepsilon_{cc} = kT$. Reprinted with permission from [26]. Copyright (2008) American Chemical Society.

single-tethered particles exhibit a much stronger small-angle peak in $S_{cc}(k)$ than two-tethered particles for all matrix polymer lengths. In addition, for $f = 1$ the small-angle peak is higher for the intermediate value of $N_m = 8$ compared with $N_m = 1$ and 50. This non-monotonicity, only seen for $f = 1$, is further discussed below. For both $f = 1$ and 2, $S_{cc}(k = 0)$ grows as $N_m$ increases similar to athermal limit results (Figure 5(b)).

We expect that microphase separation is induced primarily via clustering of nanoparticles, a signature of which is the emergence of a prominent small-angle peak in $S_{cc}(k)$. By contrast, we find (not shown) only a weak small-angle peak in the tether collective structure factor, $S_{pp}(k)$, and in the matrix polymer structure factor, $S_{mm}(k)$, for $\phi > 0.6$, and no peaks in $S_{pp}(k)$ or $S_{mm}(k)$ for $\phi < 0.6$. These differences reflect the large asymmetry of collective concentration fluctuations of the different species due to excluded volume and packing considerations, and non-zero mixture compressibility, in contrast to the essentially incompressible block copolymer melt [49]. Hence, $S_{cc}(k*)$ is employed as the order parameter to estimate the microphase separation spinodal temperatures as done for pure melts of tethered nanoparticles (Figure 4(a)).

In Figure 7, the deduced microphase spinodal temperature $T*$ ($\sim 1/\varepsilon*_{cc}$) is presented as a function of mixture composition, $\phi$, for $f = 1$, $D/d = 2$, $N_p = 8$ fillers at $\eta = 0.5$ and $\eta = 0.3$, and varying matrix polymer length. For all $N_m$, the shape of the spinodal curve for $\eta = 0.5$ (solid curves) exhibits a competition between dilution ($T*$ decreases as $\phi$ decreases) and depletion ($T*$ increases as $\phi$ decreases) behaviour. For single-tethered particles the steric hindrance due to the inter-tether repulsion is minimised, and nanoparticles can form enthalpic contacts that are further favoured via the depletion-like attractions mediated by matrix polymers as occurs in bare nanoparticle–polymer mixtures [34,35]. Note also that for $\eta = 0.5$ as the matrix polymer length increases the spinodal temperature varies non-monotonically for most $\phi$. When $0.2 \leq \phi \leq 0.6$, as $N_m$ increases from 1 to 4 the microphase spinodal temperature increases, but as $N_m$ increases from 4 to 50 we find $T*$ decreases with the highest value attained for $N_m = 4$. When $\phi < 0.2$ (system consisting of mostly polymer matrix), $T*$ decreases monotonically with increasing $N_m$. When $\phi > 0.6$ (system consisting of mostly tethered particles) the trend is not clear since the $T*$ does not vary much with $N_m$.

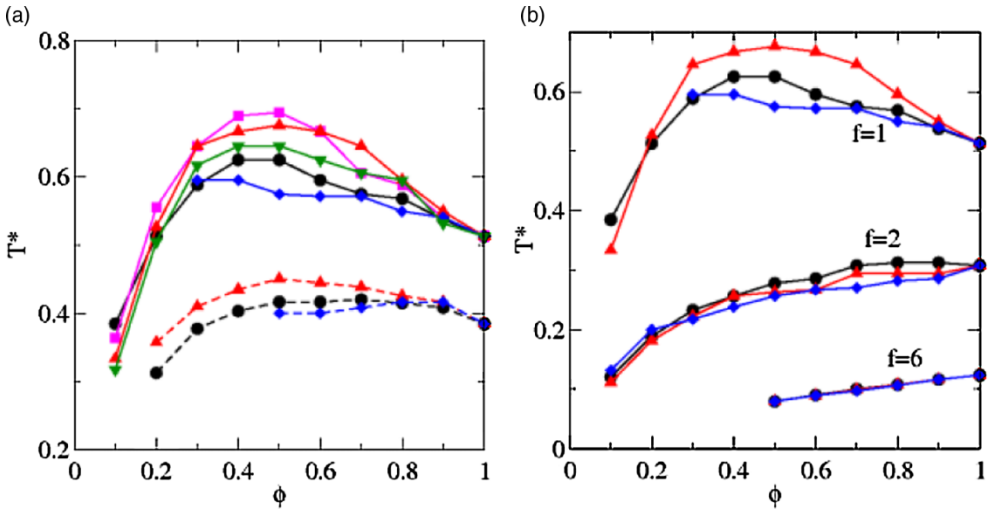


Figure 7. (a) Microphase spinodal temperature, $T^*$ ( $= 1/\varepsilon^*_{cc}$), as a function of mixture composition, $\phi$, for single-tethered particles of size $D/d = 2$ with tether length $N_p = 8$ in a polymer matrix of length $N_m = 1$ (circle), 4 (square), 8 (up triangle), 25 (down triangle) and 50 (diamond) for $\eta = 0.5$ (solid) and $\eta = 0.3$ (dashed) (for clarity the $N_m = 4$ and 25 calculations for $\eta = 0.3$ are omitted). (b) Microphase spinodal temperature as a function of mixture composition for tethered particles of size $D/d = 2$, with $f = 1$, 2 and 6 tethers of length $N_p = 8$ in a polymer matrix of length 1 (circle), 8 (up triangle) and 50 (diamond) at a packing fraction $\eta = 0.5$. Reprinted with permission from [26]. Copyright (2008) American Chemical Society.



At a packing fraction of $\eta = 0.4$ (not shown) there is a slight change in the shape of the spinodal curves, shifting towards dilution-like behaviour, while the non-monotonicity continues to exist. The value of $N_m$ at which $T^*$ is the highest is different from that for $\eta = 0.5$. At high $\phi$ ($>0.8$), the effect of $N_m$ is minimal since there is not much matrix polymer present. At intermediate $\phi$ ($0.4 \leq \phi \leq 0.7$), when $N_m$ increases from 1 to 8 we find $T^*$ increases, but for $N_m > 8$ the spinodal temperature decreases with its highest value achieved for $N_m = 8$. At low $\phi$ ($<0.3$), macrophase separation occurs, and thus there is no clear trend for $T^*$ with varying $N_m$. We note that the spinodal macrophase separation transition is determined by the simultaneous divergence of all partial collective structure factors at zero wave vector, i.e. $S_{ij}(k = 0) \rightarrow \infty$.

At a lower packing fraction of $\eta = 0.3$ (dashed lines in Figure 7(a)), the shape of the spinodal curves become more dilution-like and the microphase spinodal temperature decreases. The non-monotonic behaviour, with $T^*$ being the highest for an intermediate $N_m$, is still present at $\eta = 0.3$. For clarity of presentation, the $N_m = 4$ and 25 results are not shown since the non-monotonic dependence of $T^*$ on $N_m$ is apparent from the $N_m = 1$, 8 and 50 results. This non-monotonicity is absent in simpler mean-field-like (or random phase approximation) PRISM calculations [26], which ignore the coupling of repulsive and attractive interactions on a local scale and longer wavelength concentration fluctuations. This suggests that short-range structure plays a major role in the non-monotonic microphase ordering scale behaviour via a coupling of local and macromolecular correlations [28,39–43]. Overall, for single-tethered particles in polymer matrix there is a rich competition between depletion and dilution effects.

The effect of number of tethers ($f = 1$, 2 and 6) on the microphase spinodal is shown in Figure 7(b) for nanoparticles of size $D/d = 2$, tether length $N_p = 8$, at $\eta = 0.5$. As $f$ increases, $T^*$ decreases due to enhanced steric shielding of nanoparticle close contacts (also seen for a melt of tethered particles [20,21]), the effect of matrix length $N_m$ on $T^*$ diminishes, and a strikingly more dilution-like behaviour occurs. The fact that the mean-field-like PRISM calculations (see [26]) do not predict dilution-like behaviour with increasing number of tethers suggests that its origin is coupled energetic/packing effects on the local structure of the nanoparticles that depends on interparticle attraction strength.

### 4.3 *Effect of particle size and tether length*

Figure 8(a) presents microphase spinodal curves for a larger nanoparticle of $D/d = 3$ with a single tether of length $N_p = 27$ and 8 in a polymer matrix of varying chain length at $\eta = 0.4$. We have chosen $N_p = 27$ so that the total volume of a single tether equals the nanoparticle volume. This allows a fair comparison to be made with the smaller $N_p = 8$ and $D/d = 2$ nanoparticle system under the same equal space-filling volume condition. The shape of the microphase spinodal boundary for $N_p = 27$ and $D/d = 3$ (solid curves) is similar to that for $N_p = 8$ and $D/d = 2$ at $\eta = 0.4$ (not shown). The microphase spinodal temperatures are slightly higher for $D/d = 3$ at all compositions.

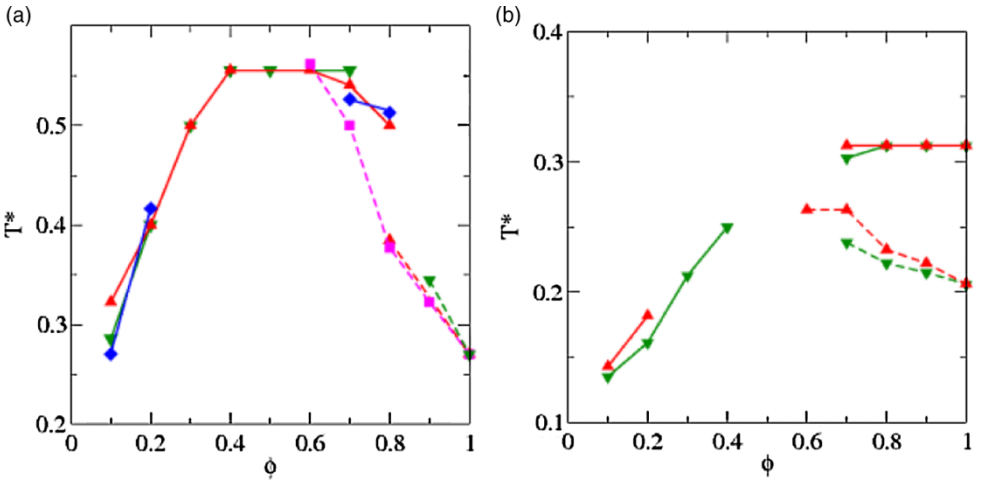


Figure 8. Microphase spinodal temperature as a function of mixture composition for tethered particles of size $D/d = 3$ with: (a) one tether of length $N_p = 27$ (solid) in a polymer matrix of length $N_m = 8$ (up triangle), 27 (down triangle) and 50 (diamond), and one tether of length $N_p = 8$ (dashed) in a polymer matrix of length $N_m = 4$ (square), 8 (up triangle) and 25 (down triangle); (b) two tethers of length $N_p = 27$ (solid) in a polymer matrix of length 8 (up triangle) and 27 (down triangle), and $N_p = 8$ (dashed) in a polymer matrix of length 8 (up triangle) and 25 (down triangle). Reprinted with permission from [26]. Copyright (2008) American Chemical Society.



Unlike the smaller single-tethered particle, which exhibited a non-monotonic dependence of $T^*$ on matrix polymer length, the value of $N_m$ does not have any effect on the spinodal temperatures for the larger single-tethered particles. However, by simply decreasing the tether length from $N_p = 27–8$, while maintaining constant particle size at $D/d = 3$ (dashed curves in Figure 8(a)), the shape of the spinodal curves is completely changed. Macrophase separation now occurs at all $\phi < 0.6$ for matrix polymer length $N_m = 4$, at all $\phi < 0.8$ for $N_m = 8$, and at all $\phi < 0.9$ for $N_m = 25$. Thus, the range of compositions, where macrophase separation occurs, significantly increases with matrix polymer length.

The results in Figure 8(a) suggest that for single-tethered particles in a polymer melt with fixed chain length, as the tether length is decreased ($N_p = 27–8$) at a constant particle size ($D/d = 3$), or the particle size is increased ($D/d = 2–3$) at a constant tether length ($N_p = 8$), the tendency for macrophase separation increases. In melts of single-tethered particles [20], a similar trend of increasing macrophase separation with increasing particle size at constant tether length is found (briefly discussed in Section 3.2). This trend occurs because as the nanoparticle volume becomes much larger than the tether volume, the effectiveness of grafted chains in promoting dispersion diminishes and macrophase separation is favoured. The presence of a homopolymer matrix enhances this macrophase separation tendency via the entropic depletion-like attraction.

Figure 8(b) presents analogous results for two-tethered nanoparticles. The shape of the microphase spinodal curves is again completely changed by simply decreasing the tether length from $N_p = 27$ (solid lines) to $N_p = 8$ (dashed lines) when $D/d = 3$. The gaps in the spinodal curves, especially at $0.3 < \phi < 0.7$, occur since we were unable to numerically converge the integral equations to an extent that allows calculation of the spinodal temperatures at those compositions. An interesting feature in Figure 8(b) is that the change in $T^*$ with decreasing $N_p$ is smaller for the two tether particles compared with the $f = 1$ analogues. This suggests that increasing the number of tethers reduces the effect of particle size and tether length on the microphase spinodal curves.

## 5. Conclusion

We have generalised the PRISM liquid-state theory to study, for the first time, the structural correlations and phase behaviour of polymer-grafted spherical nanoparticles (fillers) both in the absence [20,21] and the presence of a homopolymer melt (matrix) [26]. The interactions and model adopted mimic a system, where the matrix and grafted homopolymers are the same chemistry, nanoparticle–homopolymer and homopolymer–homopolymer attractions are weak and similar, and nanoparticles have a different chemistry from the polymer chains, resulting in unbalanced van der Waals attractions between the particles. In the absence of a polymer matrix, melts and dense solutions of nanoparticles with one, two and four chain grafts [20,21] display a system-specific power-law dependence of the microphase spinodal temperature on packing fraction. We compared the microphase spinodal curve for particles with one polymer tether [20] to the order–disorder transition curve deduced from large-scale simulations [14] and found the agreement to be surprisingly good. In the presence of a polymer matrix,

the grafted polymer (tether) and attractive nanoparticles experience clustering and/or microphase separation determined by a competition between tether repulsion and interparticle attraction, and 'depletion-like' macrophase separation induced by the homopolymer matrix. Overall, the structural organisation is dictated by a rich and subtle competition between dilution-like and depletion-like effects, which is dependent on the system parameters and hybrid filler architecture.

PRISM theory is computationally less demanding than simulations, which is especially important for systems at high volume fractions of primary interest to us. Of course, simulations have the powerful advantage of being able to predict and visualise ordered phases in contrast to homogeneous phase liquid-state PRISM theory, which describes only a generic tendency for micro- or macrophase separation. This limitation can potentially be relaxed by combining liquid-state structural information with thermodynamic density functional methods [29,32], although this has not been achieved to date for microphase separation of polymer-grafted nanoparticles. Unlike mean field theory, the PRISM approach includes concentration fluctuations on all length scales, which is often essential to capture important and subtle physical effects. Another advantage of liquid-state theory is that it provides all the intermolecular pair correlation functions and the collective structure factors (accessible to scattering experiments) over all length scales and wave vectors. Unfortunately, the present lack of experimental results for polymer-tethered particles with one or two polymer tethers dissolved in a dense polymer melt precludes critically testing the accuracy of our theory. There are preliminary experiments on six-tethered silica particles (albeit with larger nanoparticles) in a homopolymer melt of matched chemistry by Kumar and coworkers [59], and a detailed PRISM study of this system will be presented in a future publication.

To date, we have ignored non-ideal conformational effects. Although a reasonable first approximation at high melt-like volume fractions in the absence of all matrix polymer and tether polymer attractive interactions, this approximation could potentially bias the predicted local structure of some systems. New simulation results for the real space correlations and Fourier space structure factors of single- and two-tethered particles dissolved in a dense polymer melt are needed to provide critical benchmarks for the theory. Finally, PRISM theory can also treat physical and chemical heterogeneities of nanoparticles (e.g. non-spherical fillers, Janus-like spherical particles) and/or more complex polymer matrices (e.g. blends, copolymers). Its ability to compute intermolecular structural correlations, especially at small distances or large wave vectors, raises the possibility of addressing dynamical phenomena such as glass and gel formation within the framework of mode coupling [30,31,60,61] and beyond [62–64] statistical dynamical approaches.



## Acknowledgements

This work was performed at the University of Illinois and was supported by the Nanoscience and Engineering Initiative of National Science Foundation under award number DMR-0642573, and the United States Department of Energy, Basic Energy Sciences, Division of Materials Science and Engineering under contract with UT-Battelle, LLC, via Oak Ridge National Laboratory.

## References

[1] R. Krishnamoorti and R.A. Vaia, *Polymer nanocomposites*, J. Polym. Sci. B – Polym. Phys. 45 (2007), pp. 3252–3256.
[2] K.I. Winey and R.A. Vaia, *Polymer nanocomposites*, MRS Bull. 32(4) (2007), pp. 314–319.
[3] Q. Lan, L.F. Francis, and F.S. Bates, *Silica nanoparticles dispersions in homopolymer versus block copolymer*, J. Polym. Sci. B – Polym. Phys. 45 (2007), pp. 2284–2299.
[4] N. Tsubokawa, *Surface grafting of polymers onto nanoparticles in a solvent-free dry-system and applications of polymer-grafted nanoparticles as novel functional hybrid materials*, Polym. J. 39(10) (2007), pp. 983–1000.
[5] V. Goel, T. Chatterjee, L. Bombalski, K. Yurekli, K. Matyjaszewski, and R. Krishnamoorti, *Viscoelastic properties of silica-grafted poly(styrene–acrylonitrile) nanocomposites*, J. Polym. Sci. B – Polym. Phys. 44(14) (2006), pp. 2014–2023.
[6] E.P.K. Currie, W. Norde, and M.A.C. Stuart, *Tethered polymer chains: surface chemistry and their impact on colloidal and surface properties*, Adv. Colloid Interf. Sci. 100 (2003), pp. 205–265.
[7] S. Westenhoff and N.A. Kotov, *Quantum dot on a rope*, J. Am. Chem. Soc. 124(11) (2002), pp. 2448–2449.
[8] T. Song, S. Dai, K.C. Tam, S.Y. Lee, and S.H. Goh, *Aggregation behavior of two-arm fullerene-containing poly(ethylene oxide)*, Polymer 44 (2003), pp. 2529–2536.
[9] T. Song, S. Dai, K.C. Tam, S.Y. Lee, and S.H. Goh, *Aggregation behavior of C60-end-capped poly(ethylene oxide)s*, Langmuir 19 (2003), pp. 4798–4803.
[10] B. Li and C.Y. Li, *Immobilizing Au nanoparticles with polymer single crystals, patterning and asymmetric functionalization*, J. Am. Chem. Soc. 129 (2007), pp. 12–13.
[11] T. Kawauchi, J. Kumaki, and E. Yashima, *Synthesis, isolation via self-assembly, and single-molecule observation of a [60]-fullerene-end-capped isotactic poly(methyl methacrylate)*, J. Am. Chem. Soc. 127 (2005), pp. 9950–9951.
[12] E.R. Chan, L.C. Ho, and S.C. Glotzer, *Computer simulations of block copolymer tethered nanoparticle self-assembly*, J. Chem. Phys. 125 (2006), 064905.
[13] C.R. Iacovella, M.A. Horsch, Z. Zhang, and S.C. Glotzer, *Phase diagrams of self-assembled mono-tethered nanospheres from molecular simulation and comparison to surfactants*, Langmuir 21 (2005), pp. 9488–9494.
[14] C.R. Iacovella, A.S. Keys, M.A. Horsch, and S.C. Glotzer, *Icosahedral packing of polymer-tethered nanospheres and stabilization of the gyroid phase*, Phys. Rev. E 75(4) (2007), 040801.
[15] M.A. Horsch, Z.L. Zhang, and S.C. Glotzer, *Self-assembly of polymer-tethered nanorods*, Phys. Rev. Lett. 95(5) (2005), 056105.
[16] M.A. Horsch, Z.L. Zhang, and S.C. Glotzer, *Simulation studies of self-assembly of end-tethered nanorods in solution and role of rod aspect ratio and tether length*, J. Chem. Phys. 125(18) (2006), 184903.
[17] M.A. Horsch, Z. Zhang, and S.C. Glotzer, *Self-assembly of laterally-tethered nanorods*, Nano Letters 6(11) (2006), pp. 2406–2413.
[18] X. Zhang, Z.L. Zhang, and S.C. Glotzer, *Simulation study of cyclic-tethered nanocube self-assemblies: effect of tethered nanocube architectures*, Nanotechnology 18(11) (2007), 115706.
[19] J.Y. Lee, A.C. Balazs, R.B. Thompson, and R.M. Hill, *Self-assembly of amphiphilic nanoparticle-coil 'tadpole' macromolecules*, Macromolecules 37 (2004), pp. 3536–3539.
[20] A. Jayaraman and K.S. Schweizer, *Structure and assembly of dense solutions and melts of single tethered nanoparticles*, J. Chem. Phys. 128 (2008), 164904.

[21] A. Jayaraman and K.S. Schweizer, *Effect of the number and placement of polymer tethers on the structure of dense solutions of hybrid nanoparticles*, Langmuir 24(19) (2008), pp. 11119–11130.
[22] O.D. Velev, P.M. Tessier, A.M. Lenhoff, and E.W. Kaler, *Materials – A class of porous metallic nanostructures*, Nature 401(6753) (1999), p. 548.
[23] A.S. Arico, P. Bruce, B. Scrosati, J.M. Tarascon, and W. Van Schalkwijk, *Nanostructured materials for advanced energy conversion and storage devices*, Nat. Mat. 4(5) (2005), pp. 366–377.
[24] G.F. Zheng, F. Patolsky, Y. Cui, W.U. Wang, and C.M. Lieber, *Multiplexed electrical detection of cancer markers with nanowire sensor arrays*, Nat. Biotechnol. 23(10) (2005), pp. 1294–1301.
[25] D.J. Maxwell, J.R. Taylor, and S. Nie, *Self-assembled nanoparticle probes for recognition and detection of biomolecules*, J. Am. Chem. Soc. 124 (2002), pp. 9606–9612.
[26] A. Jayaraman and K.S. Schweizer, *Effective interactions, structure and phase behavior of lightly-tethered nanoparticles in a polymer melt*, Macromolecules 41(23) (2008), pp. 9430–9438.
[27] K.S. Schweizer and J.G. Curro, *PRISM theory of the structure, thermodynamics, and phase-transitions of polymer liquids and alloys*, Adv. Polym. Sci. 116 (1994), pp. 319–377.
[28] K.S. Schweizer and J.G. Curro, *Integral equation theories of the structure, thermodynamics, and phase transitions of polymer fluids*, Adv. Chem. Phys. 98 (1997), pp. 1–142.
[29] J.P. Hansen and I.R. McDonald, *Theory of Simple Liquids*, 2nd ed., Academic Press, London, 1986.
[30] W. Gotze and L. Sjogren, *Relaxation processes in supercooled liquids*, Rep. Progr. Phys. 55(3) (1992), pp. 241–376.
[31] S.P. Das, *Mode-coupling theory and the glass transition in supercooled liquids*, Rev. Mod. Phys. 76(3) (2004), pp. 785–851.
[32] S.K. Nath, J.D. McCoy, J.G. Curro, and R.S. Saunders, *The ordering of symmetric diblock copolymers: a comparison of self-consistent-field and density functional approaches*, J. Chem. Phys. 106(5) (1997), pp. 1950–1960.
[33] D. Henderson, D.M. Duh, X.L. Chu, and D. Wasan, *An expression for the dispersion force between colloidal particles*, J. Colloid Interf. Sci. 185(1) (1997), pp. 265–268.
[34] J.B. Hooper, K.S. Schweizer, T.G. Desai, R. Koshy, and P. Keblinski, *Structure, surface excess and effective interactions in polymer nanocomposite melts and concentrated solutions*, J. Chem. Phys. 121(14) (2004), pp. 6986–6997.
[35] J.B. Hooper and K.S. Schweizer, *Contact aggregation, bridging, and steric stabilization in dense polymer–particle mixtures*, Macromolecules 38 (2005), pp. 8858–8869.
[36] J.B. Hooper and K.S. Schweizer, *Theory of phase separation in polymer nanocomposites*, Macromolecules 39 (2006), pp. 5133–5142.
[37] L.M. Hall and K.S. Schweizer, *Many body effects on the phase separation and structure of dense polymer–particle melts*, J. Chem. Phys. 128 (2008), 234901.
[38] D. Chandler and H.C. Andersen, *Optimized cluster expansions for classical fluids. 2. Theory of molecular liquids*, J. Chem. Phys. 57(5) (1972), pp. 1930–1937.
[39] M. Guenza and K.S. Schweizer, *Fluctuation effects in diblock copolymer fluids: comparison of theories and experiment*, J. Chem. Phys. 106(17) (1997), pp. 7391–7410.
[40] M. Guenza and K.S. Schweizer, *Local and microdomain concentration fluctuation effects in block copolymer solutions*, Macromolecules 30 (1997), pp. 4205–4219.
[41] E.F. David and K.S. Schweizer, *Integral equation theory of block copolymer liquids I. General formalism and analytic predictions for symmetric copolymers*, J. Chem. Phys. 100(10) (1994), pp. 7767–7783.
[42] E.F. David and K.S. Schweizer, *Integral-equation theory of block-copolymer liquids. 2. Numerical results for finite hard-core diameter chains*, J. Chem. Phys. 100(10) (1994), pp. 7784–7795.
[43] E.F. David and K.S. Schweizer, *Liquid state theory of thermally driven segregation of conformationally asymmetric diblock copolymer melts*, Macromolecules 30(17) (1997), pp. 5118–5132.
[44] D.R. Heine, G.S. Grest, and J.G. Curro, *Structure of polymer melts and blends: Comparison of integral equation theory and computer simulations*, *Advanced Computer Simulation Approaches for Soft Matter Sciences I*, Vol. 173, Advances in Polymer Science, Springer, Berlin, 2005, pp. 209–249.
[45] A.C. Hindmarsh, P.N. Brown, K.E. Grant, S.L. Lee, R. Serban, D.E. Shumaker, and C.S. Woodward, *SUNDIALS: suite of nonlinear and differential/algebraic equation solvers*, ACM Trans. Math. Software 31(3) (2005), pp. 363–396.
[46] K.A. Kolbet and K.S. Schweizer, *Real space structure of associating polymer melts*, Macromolecules 33(4) (2000), pp. 1443–1458.
[47] K.A. Kolbet and K.S. Schweizer, *Microdomain scale organization and scattering patterns of associating polymer melts*, Macromolecules 33(4) (2000), pp. 1425–1442.
[48] F.S. Bates and G.H. Fredrickson, *Block copolymer thermodynamics – Theory and experiment*, Annu. Rev. Phys. Chem. 41 (1990), pp. 525–557.
[49] L. Leibler, *Theory of microphase separation in block copolymers*, Macromolecules 13 (1980), pp. 1602–1617.
[50] G.H. Fredrickson and E. Helfand, *Fluctuation effects in the theory of microphase separation in block copolymers*, J. Chem. Phys. 87(1) (1987), pp. 697–705.
[51] S. Abbas and T.P. Lodge, *Depletion interactions: a new control parameter for the self-assembly of diblock copolymer micelles*, Phys. Rev. Lett. 99 (2007), 137802.
[52] E.E. Dormidontova and T.P. Lodge, *The order–disorder transition and the disordered micelle regime in sphere forming block copolymer melts*, Macromolecules 34 (2001), pp. 9143–9155.
[53] M.J. Park, K. Char, J. Bang, and T.P. Lodge, *Order–disorder transition and critical micelle temperature in concentrated block copolymer solutions*, Macromolecules 38(6) (2005), pp. 2449–2459.
[54] T.P. Lodge, C. Pan, X. Jin, Z. Liu, J. Zhao, W.W. Maurer, and F.S. Bates, *Failure of the dilution approximation in block–copolymer solutions*, J. Polym. Sci. B – Polym. Phys. 33(16) (1995), pp. 2289–2293.
[55] F.W. Starr, J.F. Douglas, and S.C. Glotzer, *Origin of particle clustering in a simulated polymer nanocomposite and its impact on rheology*, J. Chem. Phys. 119(3) (2003), pp. 1777–1788.
[56] C.M. Wijmans, F.A.M. Leermakers, and G.J. Fleer, *Pair potentials between polymer-coated mesoscopic particles*, Langmuir 10(12) (1994), pp. 4514–4516.
[57] K.R. Shull, *Theory of end-adsorbed polymer brushes in polymeric matrices*, J. Chem. Phys. 94(8) (1991), pp. 5723–5738.
[58] T.A. Witten, L. Leibler, and P.A. Pincus, *Stress-relaxation in the lamellar copolymer mesophase*, Macromolecules 23(3) (1990), pp. 824–829.
[59] P. Akcora, H. Liu, S.K. Kumar, Y. Li, B.C. Benicewicz, L.S. Schadler, D. Acehan, A.Z. Panagiotopoulos, and J.F. Douglas, *Anisotropic self-assembly of polymer-decorated spherical nanoparticles*, Nat. Mat. (2008), in press.
[60] J. Bergenholtz, W.C.K. Poon, and M. Fuchs, *Gelation in model colloid–polymer mixtures*, Langmuir 19(10) (2003), pp. 4493–4503.
[61] Y.L. Chen and K.S. Schweizer, *Microscopic theory of gelation and elasticity in polymer–particle suspensions*, J. Chem. Phys. 120(15) (2004), pp. 7212–7222.
[62] Y.L. Chen, V. Kobelev, and K.S. Schweizer, *Barrier hopping, viscous flow, and kinetic gelation in particle–polymer suspensions*, Phys. Rev. E 71(4) (2005), 041405.
[63] K.S. Schweizer and E.J. Saltzman, *Entropic barriers, activated hopping, and the glass transition in colloidal suspensions*, J. Chem. Phys. 119(2) (2003), pp. 1181–1196.
[64] K.S. Schweizer, *Derivation of a microscopic theory of barriers and activated hopping transport in glassy liquids and suspensions*, J. Chem. Phys. 123(24) (2005), 244501.